

Water Oxidation Intermediates Applied to Catalysis: Benzyl Alcohol Oxidation

Aaron K. Vannucci, Jonathan F. Hull, Zuofeng Chen, Robert A. Binstead, Javier J. Concepcion, and Thomas J. Meyer*

Department of Chemistry, University of North Carolina at Chapel Hill, Chapel Hill, North Carolina 27599, United States

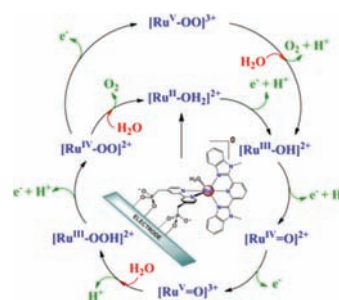
S Supporting Information

ABSTRACT: Four distinct intermediates, $\text{Ru}^{\text{IV}}=\text{O}^{2+}$, $\text{Ru}^{\text{IV}}(\text{OH})^{3+}$, $\text{Ru}^{\text{V}}=\text{O}^{3+}$, and $\text{Ru}^{\text{V}}(\text{OO})^{3+}$, formed by oxidation of the catalyst $[\text{Ru}(\text{Mebimpy})(4,4'-((\text{HO})_2\text{OPCH}_2)_2\text{-bpy})(\text{OH}_2)]^{2+}$ [Mebimpy = 2,6-bis(1-methylbenzimidazol-2-yl)] and $4,4'-((\text{HO})_2\text{OPCH}_2)_2\text{bpy}$ = 4,4'-bismethylenephosphonato-2,2'-bipyridine] on *nanoITO* (1- PO_3H_2) have been identified and utilized for electrocatalytic benzyl alcohol oxidation. Significant catalytic rate enhancements are observed for $\text{Ru}^{\text{V}}(\text{OO})^{3+}$ (~3000) and $\text{Ru}^{\text{IV}}(\text{OH})^{3+}$ (~2000) compared to $\text{Ru}^{\text{IV}}=\text{O}^{2+}$. The appearance of an intermediate for $\text{Ru}^{\text{IV}}=\text{O}^{2+}$ as the oxidant supports an O-atom insertion mechanism, and H/D kinetic isotope effects support net hydride-transfer oxidations for $\text{Ru}^{\text{IV}}(\text{OH})^{3+}$ and $\text{Ru}^{\text{V}}(\text{OO})^{3+}$. These results illustrate the importance of multiple reactive intermediates under catalytic water oxidation conditions and possible control of electrocatalytic reactivity on modified electrode surfaces.

An impressive scope of oxidative reactivity has been identified for high oxidation state Ru oxo complexes, including a family of single-site water oxidation catalysts based on $\text{Ru}^{\text{V}}=\text{O}^{3+}$ polypyridyl complexes, for which mechanisms of water oxidation have been elucidated.¹ Related single-site catalysts with phosphonate ($-\text{PO}_3\text{H}_2$)-modified ligands have been shown to function as water oxidation electrocatalysts when bound to planar ITO ($\text{Sn}(\text{IV})$ -doped In_2O_3) and FTO (fluorine-doped SnO_2) electrodes² and, more recently, to films of nanostructured ITO (*nanoITO*).^{3,4} Surface attachment can be useful in avoiding over oxidation⁵ and mechanistically insightful due to the absence of diffusion of the catalyst.⁵ Surface attachment also provides an interfacial configuration appropriate for catalytic, electrocatalytic, fuel cell, and photoelectrocatalytic applications.⁶

The mechanism of interfacial water oxidation by $[\text{Ru}(\text{Mebimpy})(4,4'-((\text{HO})_2\text{OPCH}_2)_2\text{bpy})(\text{OH}_2)]^{2+}$ (1- PO_3H_2) [Mebimpy = 2,6-bis(1-methylbenzimidazol-2-yl)] and $4,4'-((\text{HO})_2\text{OPCH}_2)_2\text{bpy}$ = 4,4'-bismethylenephosphonato-2,2'-bipyridine] bound to ITO and *nanoITO* electrodes^{2,6,7} is shown in Scheme 1. Key elements in the mechanism include stepwise proton-coupled electron transfer (PCET) oxidation from *nanoITO*| $\text{Ru}-\text{OH}_2^{2+}$ to higher oxidation states $\text{Ru}^{\text{IV}}=\text{O}^{2+}$ and $\text{Ru}^{\text{V}}=\text{O}^{3+}$. This process occurs through $\text{Ru}^{\text{III}}-\text{OH}_2^{2+}$ or $\text{Ru}^{\text{III}}-\text{OH}_2^{3+}$, with $\text{p}K_a = 2.3$ for the latter. In acidic solutions, oxidative activation from $\text{Ru}^{\text{III}}-\text{OH}_2^{2+}/\text{Ru}^{\text{III}}-\text{OH}_2^{3+}$ occurs through $\text{Ru}^{\text{IV}}(\text{OH})^{3+}$.^{7,8} Further oxidation to $\text{Ru}^{\text{V}}=\text{O}^{3+}$ followed by

Scheme 1. Water Oxidation Mechanism for *nanoITO*|1- PO_3H_2



O-atom transfer from H_2O gives $\text{Ru}^{\text{III}}-\text{OOH}^{3+}$, which can be further oxidized to the peroxide $\text{Ru}^{\text{IV}}(\text{OO})^{2+}$ followed by slow O_2 evolution. Additional oxidation of the Ru^{IV} peroxide to $\text{Ru}^{\text{V}}(\text{OO})^{3+}$ increases the lability of O_2 , leading to re-entry into the catalytic cycle through O_2 loss and regeneration of $\text{Ru}^{\text{III}}-\text{OH}_2^{2+}$. Evidence has been obtained for intermediate $\text{Ru}^{\text{IV}}(\text{OO})^{2+}/\text{Ru}^{\text{III}}-\text{OOH}^{2+}$ and $\text{Ru}^{\text{III}}-\text{OOH}^{2+}/\text{Ru}^{\text{II}}(\text{HOOH})^{2+}$ couples both in solution and on electrode surfaces.^{2,7,9}

Any mechanism for water oxidation near the thermodynamic potential for the $\text{H}_2\text{O}/\text{O}_2$ couple is necessarily complex due to the requirement for $4e^-/4\text{H}^+$ loss and O–O bond formation. Mechanistic complexity, however, creates an opportunity to examine intermediates that appear in the catalytic cycle, $\text{Ru}^{\text{IV}}=\text{O}^{2+}$, $\text{Ru}^{\text{IV}}(\text{OH})^{3+}$, $\text{Ru}^{\text{V}}=\text{O}^{3+}$, and $\text{Ru}^{\text{V}}(\text{OO})^{3+}$, for possible catalytic activity. We show here that all four have catalytic reactivity toward benzyl alcohol (BnOH), which is chosen as a model substrate. The advantages of surface-bound catalysis are exploited to identify and utilize conditions that allow for the reactivity of each to be evaluated.

Figure 1 shows cyclic voltammograms (CVs) of *nanoITO*|1- PO_3H_2 at pH 5 before and after entry into a water oxidation cycle. Limiting the potential scan to <1.35 V avoids the water oxidation cycle, which occurs following $\text{Ru}^{\text{IV}}=\text{O}^{2+} \rightarrow \text{Ru}^{\text{V}}=\text{O}^{3+}$ oxidation at $E_{\text{p,a}} \approx 1.5$ V. Oxidative peak currents for the $\text{Ru}^{\text{II}}-\text{OH}_2^{2+} \rightarrow \text{Ru}^{\text{III}}-\text{OH}_2^{2+}$ oxidation wave at $E_{1/2} = 0.75$ V vary linearly with scan rate, ν , as expected for a surface-bound couple.⁸ At scan rates <5 mV/s, integrated peak currents for the $\text{Ru}^{\text{III}}-\text{OH}_2^{2+}/\text{Ru}^{\text{IV}}=\text{O}^{2+}$ wave are comparable to those for the $\text{Ru}^{\text{II}}-\text{OH}_2^{2+}/\text{Ru}^{\text{III}}-\text{OH}_2^{2+}$ couple. At scan rates >10 mV/s, the anodic peak current, $i_{\text{p,a}}$, for the PCET process $\text{Ru}^{\text{III}}-\text{OH}_2^{2+} \rightarrow \text{Ru}^{\text{IV}}=\text{O}^{2+}$

Received: November 22, 2011

Published: February 6, 2012

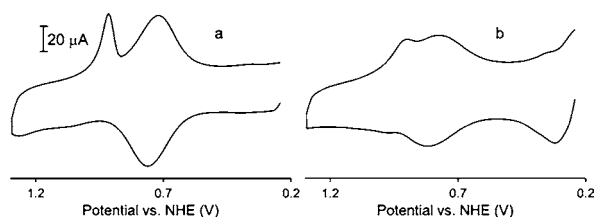


Figure 1. CVs of *nanoITO|I-PO₃H₂* at 30 mV s⁻¹ at pH 5 (*I* = 0.064 M acetate anion (OAc⁻)). (a) *nanoITO|I-PO₃H₂* before water oxidation. The wave for the thermodynamic formation of Ru^{IV}=O²⁺ at *E*_{p,a} ≈ 1.0 V is only slightly discernible, followed by the wave for the Ru^{IV}(OH)³⁺/Ru^{III}-OH²⁺ couple at *E*_{p,a} = 1.24 V. (b) *nanoITO|I-PO₃H₂* after scans to 1.5 V through the water oxidation cycle. The new waves at *E*_{1/2} = 0.34 and 0.25 V arise from a peroxide intermediate (see text).

decreases as a new wave appears at *E*_{1/2} = 1.24 V. The new wave arises from the direct oxidation of Ru^{III}-OH²⁺ in a chemically reversible but kinetically inhibited Ru^{IV}(OH)³⁺/Ru^{III}-OH²⁺ couple, which is the sole Ru(IV/III) couple observed at pH ≤ 2. As noted below, the p*K*_a for Ru^{IV}(OH)³⁺ is ~3. The skewed, narrow reduction wave observed in Figure 1a is scan rate and pH dependent and arises from the autocatalytic reduction of Ru^{IV}=O²⁺ to Ru^{III}-O⁺ followed by rapid proton transfer to give Ru^{III}-OH²⁺.⁸

The CV waveform in Figure 1a is maintained through multiple scans until the potential window is extended to 1.5 V, resulting in electrocatalytic water oxidation. After water oxidation at the interface, the waveform in Figure 1a is transformed into the waveform shown in Figure 1b. The noticeable difference between the two CVs in Figure 1 is the appearance of two new waves at *E*_{1/2} = 0.34 and 0.25 V that arise at the expense of the Ru^{III}-OH²⁺/Ru^{II}-OH₂²⁺ peak at 0.75 V. As observed in an earlier study,⁸ the new waves are due to Ru^{IV}(OO)²⁺ formation on the electrode surface and result from the pH-dependent peroxide couples Ru^{III}-OOH²⁺/Ru^{II}(HOOH)²⁺ and Ru^{IV}(OO)²⁺/Ru^{III}-OOH²⁺, which are known stable complexes.^{2,7,9} The Ru^{IV}(OO)²⁺ → Ru^V(OO)³⁺ oxidation wave occurs at ~1.3 V. These observations provide conditions for generating each of the intermediates Ru^{IV}=O²⁺, Ru^{IV}(OH)³⁺, and Ru^V(OO)³⁺ and investigating their oxidation chemistry.

Oxidation by *nanoITO|Ru^{IV}=O²⁺*. Figure 2 shows spectral changes that accompany the addition of BnOH

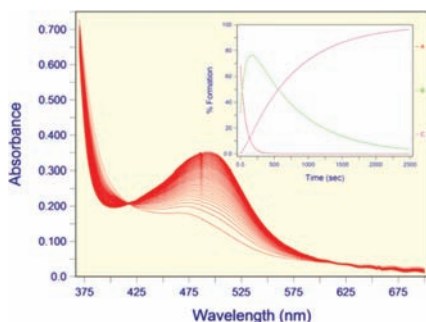
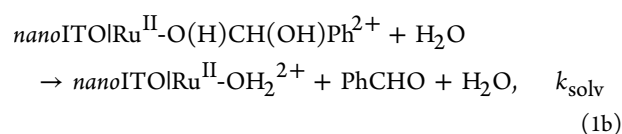
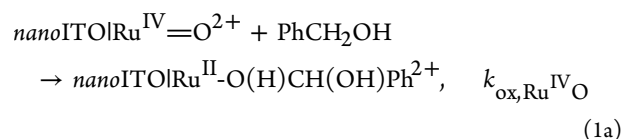


Figure 2. UV-vis monitoring of the reaction between BnOH (40 mM) and *nanoITO|Ru^{IV}=O²⁺* in pH 5, *I* = 0.064 M OAc⁻ at 23 ± 2 °C, showing the appearance of an initial intermediate at λ_{max} = 493 nm followed by *nanoITO|Ru^{II}-OH₂²⁺* at λ_{max} = 498 nm. The inset shows an analysis of the data by using a biexponential A → B → C model obtained via the software package SPECFIT/32 using normalized concentrations and an experimental time offset *t*₀ ≈ 30 s, where A is *nanoITO|Ru^{IV}=O²⁺*, B is an intermediate (see eq 1b), and C is *nanoITO|Ru^{II}-OH₂²⁺*.

(40 mM in pH 5, *I* = 0.064 M OAc⁻, 23 ± 2 °C) to a cuvette containing *nanoITO|Ru^{IV}=O²⁺*, generated by oxidation of Ru^{II}-OH₂²⁺ in a pH 9 solution of NaOCl, with the cell aligned perpendicularly to the spectrometer light-path. Characteristic spectral changes for reduction to *nanoITO|Ru^{II}-OH₂²⁺* with λ_{max} = 498 nm and isosbestic points at 614 and 423 nm occurred with addition of BnOH. Importantly, there was no spectroscopic evidence for Ru^{III}-OH²⁺ (λ_{max} = 380 nm at pH 5) or Ru^{III}-OH₂²⁺ (λ_{max} = 650 nm at pH 1) as intermediates on the surface, suggesting a concerted 2e⁻ mechanism.

Initial oxidation of Ru^{IV}=O²⁺ to the intermediate species with λ_{max} = 493 nm occurs with *k*_{ox} = (1.3 ± 0.02) × 10⁻² s⁻¹. λ_{max} then shifts with time to 498 nm, characteristic of Ru^{II}-OH₂²⁺, indicating initial formation of a Ru^{II} intermediate followed by solvolysis to give *nanoITO|Ru^{II}-OH₂²⁺*. These observations are consistent with a mechanism in which oxidation of BnOH occurs by C-H insertion to give a coordinated aldehyde hydrate, which undergoes solvolysis to give *nanoITO|Ru^{II}-OH₂²⁺* (eqs 1a,b). The same reactivity was observed for BnOH oxidation by the Ru^{IV}=O²⁺ oxidant [Ru^{IV}(tpy)(4,4'-((HO)₂OPCH₂)₂bpy)(O)]²⁺ (tpy = 2,2':6',2''-terpyridine) on TiO₂.⁶



In order to verify benzaldehyde as a major product, a controlled potential electrolysis of *nanoITO|I-PO₃H₂* in the presence of 20 mM BnOH was performed at 1.05 V with stirring for 13 h. A steady-state current density of ~8000 μA/cm³ was maintained during the electrolysis (SI). GC analysis showed that benzaldehyde was formed with a faradaic efficiency of 64%.

Oxidation by *nanoITO|Ru^{IV}(OH)³⁺*. Electrocatalytic oxidation of BnOH by *nanoITO|Ru^{IV}(OH)³⁺* was investigated by cyclic voltammetry at pH 5. As noted above, Ru^{III}-OH²⁺ → Ru^{IV}(OH)³⁺ oxidation occurs at *E*_{1/2} = 1.24 V. Further evidence for surface-bound Ru^{IV}(OH)³⁺ is shown in CVs of *nanoITO|I-PO₃H₂* at pH 1 (Figure S2), where the magnitude of *i*_{p,a} and the chemical reversibility of the Ru^{IV}(OH)³⁺/Ru^{III}-OH²⁺ couple are enhanced relative to those at pH 5.

Figure 3 shows CVs of *nanoITO|I-PO₃H₂* with increasing concentrations of BnOH. There is no evidence for the peroxide

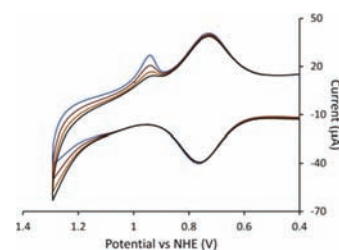


Figure 3. CVs of *nanoITO|I-PO₃H₂* at 20 mV/s (pH 5, *I* = 0.064 M OAc⁻, 23 ± 2 °C) with added increments of BnOH (2, 4, 6, and 8 mM) showing the electrocatalytic activity of Ru^{IV}(OH)³⁺.

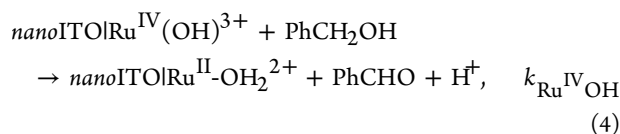
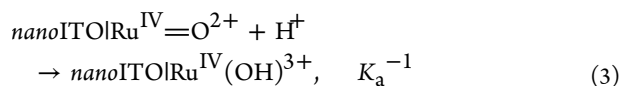
couples on the surface of the electrode under these conditions. No sign of current enhancement was observed at the potential

for the $\text{Ru}^{\text{IV}}=\text{O}^{2+}/\text{Ru}^{\text{III}}-\text{OH}^{2+}$ couple ($E_{\text{p,a}} = 1.0 \text{ V}$) on the CV time scale, consistent with the slow oxidation observed in Figure 1. This indicates that catalytic oxidation of BnOH on the CV time scale occurs from $\text{Ru}^{\text{IV}}(\text{OH})^{3+}$.

As shown in Figure S8, BnOH oxidation by *nanoITO*| $\text{Ru}^{\text{IV}}(\text{OH})^{3+}$ is acid dependent. The electrochemical kinetic measurements were repeated at 1.24 V, and k_{obs} values were obtained as a function of various acid concentrations (HNO_3) from pH 4 to 1. The dependence of k_{obs} with $[\text{H}^+]$ provides evidence for saturation at high acid concentrations, consistent with the rate law in eq 2 and the mechanism in eqs 3 and 4. In eq 2, $[\text{Ru}^{\text{IV}}_{\text{tot}}]$ is the total concentration of Ru^{IV} ($\text{Ru}^{\text{IV}}(\text{OH})^{3+}$, $\text{Ru}^{\text{IV}}=\text{O}^{2+}$), K_a is the acid dissociation constant for *nanoITO*| $\text{Ru}^{\text{IV}}(\text{OH})^{3+}$, and $k_{\text{Ru}^{\text{IV}}\text{OH}}$ is the rate constant for *nanoITO*| $\text{Ru}^{\text{IV}}(\text{OH})^{3+}$ oxidation of BnOH. Based on the inverse–inverse plot in the inset in Figure S8, $\text{p}K_a = 3.2 \pm 0.3$ for *nanoITO*| $\text{Ru}^{\text{IV}}(\text{OH})^{3+}$ and $k_{\text{Ru}^{\text{IV}}\text{OH}} = 11.1 \pm 0.4 \text{ M}^{-1} \text{ s}^{-1}$, which was confirmed by steady-state current measurements at 150 s at an applied potential of 1.24 V (SI). The number of moles of active $\text{Ru}^{\text{IV}}(\text{OH})^{3+}$ catalyst on the surface was determined by the integrated current under the $\text{Ru}^{\text{IV}}(\text{OH})^{3+}/\text{Ru}^{\text{III}}-\text{OOH}^{2+}$ wave in the absence of substrate and eq 5, where Q is the integrated charge, n is the number of electrons transferred ($=1$), F is the Faraday constant, A is the area of the electrode, and Γ is the surface coverage of active catalyst in mol/cm^2 . The remaining sites on the electrode surface (Ru^{III} and $\text{Ru}^{\text{IV}}=\text{O}^{2+}$) were assumed to be inactive.

$$\text{rate} = k_{\text{obs}}[\text{Ru}^{\text{IV}}]_{\text{tot}} \quad (2a)$$

$$k_{\text{obs}} = k_{\text{Ru}^{\text{IV}}\text{OH}} K_a [\text{BnOH}] \frac{[\text{H}^+]}{1 + K_a [\text{H}^+]} \quad (2b)$$

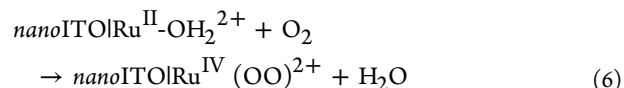


$$Q = nFA\Gamma \quad (5)$$

To gain insight into the catalytic mechanism, kinetic isotope effects (KIEs) were evaluated by measurements in D_2O and with the deuterated benzyl- d^7 alcohol, which gave $(k_{\text{H}_2\text{O}}/k_{\text{D}_2\text{O}}) = 1.1 \pm 0.1$ and $(k_{\text{C}_6\text{H}_5\text{CH}_2\text{OH}}/k_{\text{C}_6\text{D}_5\text{CD}_2\text{OH}}) = 3.0 \pm 0.2$. The magnitudes of these KIE values indicate that water plays a small role in the rate-determining step, and the C–H/C–D KIE of 3 suggests a possible hydride transfer mechanism, similar to results obtained in a previous study on a related oxidant.¹⁰ Deaeration with N_2 had no effect, ruling out a free radical mechanism involving radical capture by oxygen. Controlled potential electrolysis of *nanoITO*| $\text{Ru}^{\text{IV}}(\text{OH})^{3+}$ in the presence of 20 mM BnOH at 1.24 V for 16 h resulted in a steady-state current density of $\sim 11000 \mu\text{A}/\text{cm}^2$. Benzaldehyde was the major product (57% faradaic efficiency) as determined by GC analysis.

Oxidation by *nanoITO*| $\text{Ru}^{\text{V}}(\text{OO})^{3+}$. Catalytic rates for BnOH oxidation were further increased following an oxidative scan through the catalytic water oxidation wave, which led to the appearance of waves for the $\text{Ru}^{\text{IV}}(\text{OO})^{2+}/\text{Ru}^{\text{III}}-\text{OOH}^{2+}$ and

$\text{Ru}^{\text{III}}-\text{OOH}^{2+}/\text{Ru}^{\text{II}}(\text{HOOH})^{2+}$ couples on the electrode surface, as described above. A previous DFT study showed two possible forms for both $\text{Ru}^{\text{IV}}(\text{OO})^{2+}$ and the oxidized $\text{Ru}^{\text{V}}(\text{OO})^{3+}$: an O_2 -chelating, 7-coordinate complex for which there is literature precedence,⁹ or an “open”, 6-coordinate Ru complex with O_2^{2-} terminally bound.⁹ Slow interconversion between the two forms has been predicted.⁹ DFT calculations favor the chelate form in Ru^{IV} and the “open” form in Ru^{V} , with the latter undergoing kinetically facile O_2 release. We presume that the relatively stable peroxide intermediate observed on the electrode surface is the chelate form, $\text{Ru}^{\text{IV}}(\text{OO})^{2+}$. This form is also accessible by O_2 substitution for water in air-dried electrodes (eq 6).



The peroxide waves are persistent on the electrode surface and can be studied separately from water oxidation by limiting the potential window to $<1.34 \text{ V}$ during CV analysis. Figure 4

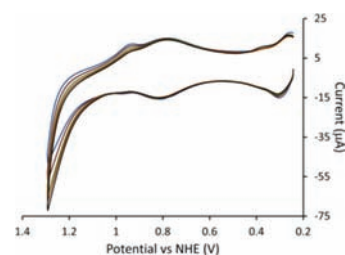
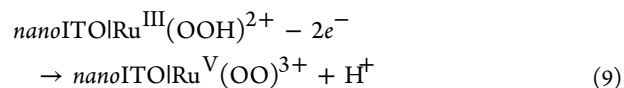
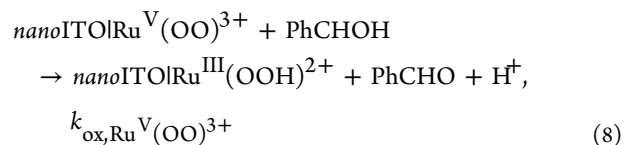


Figure 4. CVs of *nanoITO*|1- PO_3H_2 at 20 mV/s (pH 5, $I = 0.064 \text{ M OAc}^-$, $23 \pm 2 \text{ }^\circ\text{C}$), with added BnOH (2, 4, 6, and 8 mM), showing the catalytic activity of $\text{Ru}^{\text{V}}(\text{OO})^{3+}$.

shows CVs for the catalytic response of *nanoITO*| $\text{Ru}^{\text{IV}}(\text{OO})^{2+}$ in the presence of increasing amounts of BnOH. Catalytic rate constants were evaluated by steady-state current measurements after 150 s with stirring at 1.27 V by application of eq 7 to the data (SI). From the measurements, $k_{\text{Ru}^{\text{V}}(\text{OO})^{3+}} = 28.1 \pm 0.5 \text{ M}^{-1} \text{ s}^{-1}$ (pH 5, $I = 0.064 \text{ M OAc}^-$, $23 \pm 2 \text{ }^\circ\text{C}$).

$$i_{\text{cat}} = n_{\text{cat}} F A \Gamma k_{\text{ox, BnOH}} [\text{BnOH}] \quad (7)$$

Similar to $\text{Ru}^{\text{IV}}(\text{OH})^{3+}$ as the oxidant, $k_{\text{H}_2\text{O}}/k_{\text{D}_2\text{O}} = 1.1 \pm 0.1$ and $k_{\text{C}_6\text{H}_5\text{CH}_2\text{OH}}/k_{\text{C}_6\text{D}_5\text{CD}_2\text{OH}} = 2.7 \pm 0.1$, and there is a lack of dependence on O_2 for $\text{Ru}^{\text{V}}(\text{OO})^{3+}$ as the oxidant, suggesting a net hydride transfer mechanism, possibly by H-rebound. This mechanism would generate benzaldehyde and $\text{Ru}^{\text{III}}(\text{OOH})^{2+}$ that could be oxidized back into the catalytic cycle as shown in eqs 8 and 9. Controlled potential electrolysis of *nanoITO*| $\text{Ru}^{\text{V}}(\text{OO})^{3+}$ in the presence of 20 mM BnOH at 1.29 V for 16 h produced a steady-state current of $\sim 13 \text{ mA}/\text{cm}^2$, corresponding to $\sim 2400 \text{ } 2e^-$ turnovers. Benzaldehyde was the major product determined by GC analysis, with a 66% faradaic efficiency.



The Ru^V=O³⁺ form of the catalyst is also active toward electrocatalytic BnOH oxidation, but *nanoITO*Ru^V=O³⁺ is only accessible by Ru^{IV}=O²⁺→Ru^V=O³⁺ oxidation at $E_{p,a} \approx 1.5$ V. At this potential, BnOH oxidation overlaps with H₂O oxidation. The overlapping catalytic processes make a detailed analysis of BnOH oxidation by Ru^V=O³⁺ difficult in aqueous solutions. Qualitatively, oxidation currents at 1.5 V increased with increasing amounts of added BnOH, suggesting that oxidation of BzOH by *nanoITO*Ru^V=O³⁺ is comparable in rate to the oxidation of BnOH by *nanoITO*Ru^V(OO)³⁺. Currently, measurements are underway in propylene carbonate/H₂O mixtures in order to study the catalytic activity of Ru^V=O³⁺ without complication from extensive background water oxidation.

Table 1 summarizes kinetic parameters, KIE values, and turnover numbers from the controlled potential electrolysis

Table 1. Rate Constants, KIE Values, and Turnover Numbers for Ru^{IV}=O²⁺, Ru^{IV}(OH)³⁺, and Ru^V(OO)³⁺ on *nanoITO*^a

	k_{cat} M ⁻¹ s ⁻¹	KIE		
		BnOH- d_7	D ₂ O	TON ^b
<i>nanoITO</i> Ru ^V (OO) ³⁺	28.1	2.7	1.1	2440
<i>nanoITO</i> Ru ^{IV} (OH) ³⁺	11.1	3.0	1.1	400
<i>nanoITO</i> Ru ^{IV} =O ²⁺	0.01	c	c	70

^a $E^{\circ}(\text{Ru}^{\text{V}}(\text{OO})^{\text{3+}}/\text{Ru}^{\text{IV}}(\text{OOH})^{\text{2+}}) = 0.89$ V, $E^{\circ}(\text{Ru}^{\text{IV}}(\text{OH})^{\text{3+}}/\text{Ru}^{\text{II}}\text{-OH}_2^{\text{2+}}) = 0.99$ V, $E^{\circ}(\text{Ru}^{\text{IV}}=\text{O}^{\text{2+}}/\text{Ru}^{\text{II}}\text{-OH}_2^{\text{2+}}) = 0.90$ V at pH 5, $I = 0.064$ OAc⁻, 23 ± 0.2 °C. ^bMols of benzaldehyde produced from mols of catalyst on the electrode surface $\pm 10\%$. ^cNot available.

experiments. By using the advantages of the surface-bound catalyst on *nanoITO*, we have been able to identify and exploit a series of high oxidation state intermediates found in water oxidation cycles. These results are remarkable in illustrating a cascading increase in reactivity by over a factor of ~ 3000 for BnOH oxidation by a single catalytic system with E° values for $2e^-/1H^+$ couples at pH 5 that vary by only ~ 0.1 V. The appearance of contributions to BnOH oxidation by four different forms of the same catalyst, Ru^V=O³⁺, Ru^V(OO)³⁺, Ru^{IV}(OH)³⁺, and Ru^{IV}=O²⁺, also raises a warning flag about interpreting data on oxo-catalyzed oxidations with excess oxidants, notably ceric ammonium sulfate. Under these conditions, with added water, there could be contributions from several forms of the catalyst.

Detailed mechanistic analyses are currently under investigation, but there are indications of what may be exploitable mechanistic diversity. Ru^{IV}=O²⁺ oxidizes BnOH through a discrete intermediate, presumably by C–H insertion. The appearance of moderate C–H/C–D KIE values and the absence of an O₂ effect point to hydride transfer or H-atom rebound mechanisms for *nanoITO*Ru^{IV}(OH)³⁺ and *nanoITO*Ru^V(OO)³⁺. Such pathways [e.g., Ru^{IV}(OH)³⁺ + PhCH₂OH → Ru^{II}-OH₂²⁺ + PhCHOH⁺; Ru^V(OO)³⁺ + PhCH₂OH → Ru^{III}-OOH²⁺ + PhCHOH⁺] are appealing because they avoid high-energy radical intermediates.

■ ASSOCIATED CONTENT

● Supporting Information

Additional information as noted in the text. This material is available free of charge via the Internet at <http://pubs.acs.org>.

■ AUTHOR INFORMATION

Corresponding Author

tjmeyer@email.unc.edu

Notes

The authors declare no competing financial interest.

■ ACKNOWLEDGMENTS

Funding by the Center for Catalytic Hydrocarbon Functionalization, an Energy Frontier Research Center (EFRC) funded by the U.S. Department of Energy (DOE), Office of Science, Office of Basic Energy Sciences, under Award DE-SC0001298 supporting J.F.H. and the electrochemical experiments of A.K.V. and the UNC EFRC Solar Fuels, an EFRC funded by the U.S. DOE, Office of Science, Office of Basic Energy Sciences, under Award DE-SC0001011 for supporting R.A.B. and J.J.C. and the material preparation performed by A.K.V. is gratefully acknowledged. Support for the purchase of the instrumentation from UNC EFRC (Solar Fuels, An EFRC funded by the U.S. DOE, Office of Science, Office of Basic Energy Sciences under Award Number DE-SC0001011) and from UNC Solar Energy Research Center Instrumentation Facility, funded by the U.S. DOE, Office of Energy Efficiency & Renewable Energy, under Award Number DE-EE0003188 are gratefully acknowledged.

■ REFERENCES

- (1) (a) Concepcion, J. J.; Jurss, J. W.; Brennaman, K. M.; de Toledo Patrocinio, A. O.; Hoertz, P. G.; Iha, N. Y. M.; Templeton, J. L.; Meyer, T. J. *Acc. Chem. Res.* **2009**, *42*, 1954. (b) Concepcion, J. J.; Jurss, J. W.; Templeton, J. L.; Meyer, T. J. *J. Am. Chem. Soc.* **2008**, *130*, 16462. (c) McDaniel, N. D.; Coughlin, F. J.; Tinker, L. L.; Bernhard, S. *J. Am. Chem. Soc.* **2008**, *130*, 210. (d) Tseng, H.-W.; Zong, R.; Muckerman, J. T.; Thummel, R. *Inorg. Chem.* **2008**, *47*, 11763. (e) Hull, J. F.; Balcells, D.; Blakemore, J. D.; Incarvito, C. D.; Eisenstein, O.; Brudvig, G. W.; Crabtree, R. H. *J. Am. Chem. Soc.* **2010**, *132*, 16094. (g) Gao, Y.; Akemark, T.; Liu, J. H.; Sun, L. C.; Akemark, B. *J. Am. Chem. Soc.* **2009**, *131*, 8726. (h) Duan, L. L.; Xu, Y. H.; Zhang, P.; Wang, M.; Sun, L. C. *Inorg. Chem.* **2010**, *49*, 209.
- (2) Chen, Z.; Concepcion, J. J.; Jurss, J. W.; Meyer, T. J. *J. Am. Chem. Soc.* **2009**, *131*, 15580.
- (3) Chen, Z.; Concepcion, J. J.; Hull, J. F.; Hoertz, P. G.; Meyer, T. J. *Dalton Trans.* **2010**, *39*, 6950.
- (4) Hoertz, P. G.; Chen, Z.; Kent, C. A.; Meyer, T. J. *Inorg. Chem.* **2010**, *49*, 8179.
- (5) Gallagher, L. A.; Meyer, T. J. *J. Am. Chem. Soc.* **2001**, *123*, 5308.
- (6) Galopponi, E. *Coord. Chem. Rev.* **2010**, *248*, 1283.
- (7) Concepcion, J. J.; Jurss, J. W.; Templeton, J. L.; Meyer, T. J. *J. Am. Chem. Soc.* **2008**, *130*, 16462.
- (8) Chen, Z.; Vannucci, A. K.; Meyer, T. J. *Proc. Natl. Acad. Sci. U.S.A.* **2011**, *108*, E1461.
- (9) Concepcion, J. J.; Tsai, M. K.; Muckerman, J. T.; Meyer, T. J. *J. Am. Chem. Soc.* **2010**, *132*, 1545.
- (10) Bryant, J. R.; Matsuo, T.; Mayer, J. M. *Inorg. Chem.* **2004**, *43*, 1587.